

## Alignment of a Model Amyloid Peptide Fragment in Bulk and at a Solid Surface

Ian W. Hamley,\* Valeria Castelletto, Claire M. Moulton, José Rodríguez-Pérez, Adam M. Squires, Tugce Eralp, and Georg Held

Department of Chemistry, University of Reading, Reading, RG6 6AD, U.K.

Matthew R. Hicks and Alison Rodger

Department of Chemistry, University of Warwick, Coventry CV4 7AL, U.K.

Received: February 13, 2010; Revised Manuscript Received: May 13, 2010

The alignment of model amyloid peptide YYKLVFFC is investigated in bulk and at a solid surface using a range of spectroscopic methods employing polarized radiation. The peptide is based on a core sequence of the amyloid  $\beta$  ( $A\beta$ ) peptide, KLVFF. The attached tyrosine and cysteine units are exploited to yield information on alignment and possible formation of disulfide or dityrosine links. Polarized Raman spectroscopy on aligned stalks provides information on tyrosine orientation, which complements data from linear dichroism (LD) on aqueous solutions subjected to shear in a Couette cell. LD provides a detailed picture of alignment of peptide strands and aromatic residues and was also used to probe the kinetics of self-assembly. This suggests initial association of phenylalanine residues, followed by subsequent registry of strands and orientation of tyrosine residues. X-ray diffraction (XRD) data from aligned stalks is used to extract orientational order parameters from the 0.48 nm reflection in the cross- $\beta$  pattern, from which an orientational distribution function is obtained. X-ray diffraction on solutions subject to capillary flow confirmed orientation in situ at the level of the cross- $\beta$  pattern. The information on fibril and tyrosine orientation from polarized Raman spectroscopy is compared with results from NEXAFS experiments on samples prepared as films on silicon. This indicates fibrils are aligned parallel to the surface, with phenyl ring normals perpendicular to the surface. Possible disulfide bridging leading to peptide dimer formation was excluded by Raman spectroscopy, whereas dityrosine formation was probed by fluorescence experiments and was found not to occur except under alkaline conditions. Congo red binding was found not to influence the cross- $\beta$  XRD pattern.

### Introduction

Alignment of self-assembled peptide structures such as  $\beta$ -sheet (“amyloid”) fibrils is important to nanobiotechnology applications. These include the development of substrates for control of cell morphology and differentiation<sup>1,2</sup> or the fabrication of aligned peptide nanowires for applications in bionanoelectronics or the templated growth of inorganic materials.<sup>3</sup>

In the present paper, the alignment of peptide YYKLVFFC in bulk and on solid surfaces is investigated and compared. We have previously reported on the self-assembly of YYKLVFFC in aqueous solution.<sup>4</sup> This peptide is based on the core sequence KLVFF<sup>5</sup> from the amyloid beta ( $A\beta$ ) peptide, which comprises residues  $A\beta$ (16–20). YYKLVFFC contains terminal tyrosine and cysteine residues to enable possible functionalization via, for instance, polymer conjugation at the C-terminal cysteine residue. The tyrosine residues also enable the introduction of responsiveness to pH, for instance, or bioconjugation,<sup>6</sup> or phosphorylation/dephosphorylation. In our previous paper,<sup>4</sup> we reported on the secondary structure as probed via CD and FTIR, with a particular emphasis on the influence of pH. Nematic phase formation was noted via observation of birefringence of samples between crossed polars and anisotropy of small-angle X-ray scattering profiles. Fibril morphology was examined by cryogenic transmission electron microscopy.

Here, peptide YYKLVFFC is used as a model peptide to investigate alignment in bulk solutions via in situ techniques, including linear dichroism, X-ray diffraction, and small-angle X-ray scattering (SAXS) on solutions of the peptides under flow. This is complemented by an investigation of alignment of dried stalks of peptide by polarized Raman spectroscopy and X-ray diffraction. Polarized Raman spectroscopy has been employed to investigate the conformation and alignment of  $\beta$ -sheet structures (for example, in silk<sup>7–9</sup>) or of  $\alpha$ -helices within virus coat proteins.<sup>10</sup> A quantitative analysis of the Raman tensor for specific units (for example, tyrosines<sup>7,11</sup>) enables information on the orientation of these with respect to the backbone to be obtained. Here, orientation within a stalk of YYKLVFFC is compared with the alignment of a film dried on silicon as studied by near-edge X-ray absorption fine structure (NEXAFS) spectroscopy. NEXAFS spectroscopy has previously been used to investigate the adsorption of self-assembling peptides.<sup>12–14</sup> However, we are not aware of previous attempts to use the method to gain information on sample alignment relative to the plane of the substrate. To confirm the nature of the self-assembled structures within the aligning fibrils, we also investigated the possible formation of peptide dimers due to disulfide bridging, or at high pH, dityrosine linking. No evidence was found for disulfide formation, as probed by Raman spectroscopy, for stalks or solutions. Dityrosine formation was investigated by fluorescence spectroscopy. The possible influence of Congo red binding on the structure and alignment of fibrils was also examined, following recent work<sup>15</sup> on the related

\* Corresponding author. Also at Diamond Light Source, Harwell Science and Innovation Campus, Didcot OX11 0DE, U.K.

peptide KLVFFAL, which forms peptide nanotubes (in water/ acetonitrile mixtures, at pH 7), in contrast to YYKLVFFC, which forms fibrils. This prior work suggested that this dye, a common diagnostic for amyloid formation, has no effect on the  $\beta$ -sheet structure.

Linear dichroism (LD) is a valuable technique to investigate alignment in real time of peptides and other biomolecules.<sup>16</sup> Here, we discuss LD data from aqueous solutions of YYKLVFFC aligned by Couette flow.<sup>17–19</sup> The differential absorption of the UV light parallel and perpendicular to the orientation axis provides information on alignment associated with specific electronic transitions from defined moieties within the sample (e.g., aromatic or carbonyl units). Small-angle X-ray scattering allows the orientation of soft materials, such as peptides in solution to be investigated in situ using appropriate flow devices, such as a Couette cell, and is used here to examine the flow-induced alignment of YYKLVFFC at the length scale of tens of nanometres.

These in situ techniques may be complemented with the study of aligned samples, prepared as stalks, from dried threads of peptide solution. We studied the alignment of a dried stalk of YYKLVFFC via X-ray diffraction (determination of the order parameter  $\bar{P}_2$  from the anisotropy of the 4.8 Å  $\beta$ -strand spacing) and polarized Raman spectroscopy. Polarized Raman spectroscopy enables the orientation of units that give rise to specific Raman bands to be determined. Here, we exploit the fact that tyrosine gives well-defined peaks in the Raman spectrum to investigate the orientation of these using polarized spectroscopy. Use of polarized Raman spectroscopy complements methods such as polarized FTIR (infrared-LD),<sup>20,21</sup> or the use of FTIR in different geometries (transmission through films on CaF<sub>2</sub> plates, as compared with grazing incidence ATR on films on gold<sup>22–24</sup>), which also provides information on alignment of specific chemical functionalities within aligned peptide assemblies. In the ATR-FTIR geometry, the peptide fibrils exhibit the same lack of in-plane order as in our NEXAFS experiments. The results from polarized Raman spectroscopy are compared with those from NEXAFS spectroscopy on dried films, performed by varying the angle of incidence of the polarized synchrotron radiation with respect to the sample surface.

## Experimental Section

**Materials.** NH<sub>2</sub>–YYKLVFFC–COOH, referred to as YYKLVFFC, was custom-synthesized by C.S. Bio Company (Menlo Park, CA) and was used as received as a TFA salt. Purity was 96.87% by HPLC in water/acetonitrile (0.1% TFA). Electrospray ionization mass spectroscopy (Bruker microTOF, BioCentre, University of Reading) confirmed (Supporting Information (SI) Figures 1 and Figure 2) a molar mass of 1082.54, consistent with the expected formula C<sub>56</sub>H<sub>75</sub>N<sub>9</sub>O<sub>11</sub>S<sub>1</sub>. Good (0.0405 sigma fit; –0.48 mDa error) correlation was observed (SI Figure 3) between acquired vs predicted isotope patterns, indicating that assignment of the chemical formula C<sub>56</sub>H<sub>75</sub>N<sub>9</sub>O<sub>11</sub>S<sub>1</sub> is a good match. No evidence for disulfide or dityrosine cross-linking was observed under the electrospray ionization conditions employed for the mass spectroscopy (vide infra).

To characterize self-assembly in water, solutions were made using amounts of peptide dissolved in Millipore water. The pH was adjusted from ~4.7 to pH 7 and pH 11 ± 0.5, with 1 M NaOH.

**Polarized Optical Microscopy.** Samples (2, 5, or 7 wt % YYKLVFFC) were stained with Congo red using a freshly prepared and filtered Congo Red/NaCl solution. The Congo Red/NaCl solution contained 0.5 wt % Congo Red and 0.2 wt %

NaCl diluted in a MeOH/water mixture (80% MeOH, 20% water).<sup>25</sup> Samples were then placed between a glass slide and a coverslip. Images were obtained using an Olympus BX41 microscope with the sample between crossed polarizers, and images were obtained with a Canon G2 digital camera.

**X-ray Diffraction (XRD).** Measurements were performed on stalks prepared by drying filaments of the peptide from 1 wt % solutions. Solutions of the peptide were suspended between the ends of wax-coated capillaries and dried. The stalks were mounted (vertically) onto the four axis goniometer of a RAXIS IV++ X-ray diffractometer (Rigaku) equipped with a rotating anode generator. The XRD data was collected using a Saturn 992 CCD camera.

**Polarized Raman Spectroscopy on a Stalk.** A stalk as prepared for XRD was used. Spectra were collected with a Renishaw inVia Reflex Raman microscope (Gloucestershire, U.K.). The excitation radiation was provided by a 785 nm diode laser (300 mW at full power). The polarization of the incident light was adjusted using a polarizer filter, and that of the scattered radiation, by using a second polarizer and a half-wave plate. The laser was focused onto the surface of the samples with a 20× objective (NA = 0.40), which also collected the Raman scattered radiation (180° backscattering geometry). Up to four accumulations of 10 s scans at 10–50% laser power were summed. No fluorescence or sample heating artifacts were observed at these conditions. The detector was a Peltier-cooled CCD array. Two spectra were acquired for each sample:  $I_{cc}$ , with the incident and scattered electric vectors parallel to the direction of sample alignment (director); and  $I_{bb}$ , with the incident and scattered electric vectors perpendicular to the director.

**Raman Spectroscopy in Solution.** Raman spectra were recorded on a Thermo scientific NXR FT-Raman module equipped with a NXR genie detector. The laser power was set at 2 W at 1064 cm<sup>-1</sup>. A spectrum was recorded for 5 wt % YYKLVFFC in water, and data was collected from 100 to 4000 cm<sup>-1</sup> with 2 cm<sup>-1</sup> intervals, taking 200 averages with baseline corrections using Omnic data analysis software.

**UV Fluorescence Spectroscopy.** Spectra were measured on a Cary Eclipse fluorescence spectrometer and samples were contained in a 1.0 cm path-length quartz cuvette. The fluorescence intensity was measured for water and 0.01% YYKLVFFC in water at pH 7 and pH 11. Emission spectra were recorded by excitation at 320 nm (slit width of 5 nm) from 340 to 600 nm, taking 20 averages at room temperature, and the background was subtracted. Excitation spectra were also measured at 410 nm (slit width of 5 nm) from 250 to 410 nm, taking 20 averages at room temperature, and the background was subtracted.

**Flow-Aligning X-ray Diffraction.** A capillary flow device was used, details of which have been given elsewhere.<sup>26</sup> Briefly, the central part of the capillary flow device is a computer-controlled peristaltic pump that allows controlled volume and time dispensing. The flow rate is recorded and the unit is interfaced to a PC for acquisition of flow rate data. We used borosilicate capillaries with  $D = 1$  mm internal diameter and 0.01 mm wall thickness. The measured flow rates were in the range  $Q = 1–6$  mL min<sup>-1</sup>. These correspond to Newtonian shear rates at the wall of  $\dot{\gamma} = 32Q/\pi R^3 = 170–1020$  s<sup>-1</sup>. The actual flow rate will differ for non-Newtonian fluids, and for this reason, we quote flow rates  $Q$ . The XRD experiments were carried out using a four axis goniometer of a RAXIS IV++ X-ray diffractometer (Rigaku) equipped with a rotating anode generator. The XRD data was collected using a Saturn 992 CCD camera. The sample–detector distance was 90 or 95 mm. The

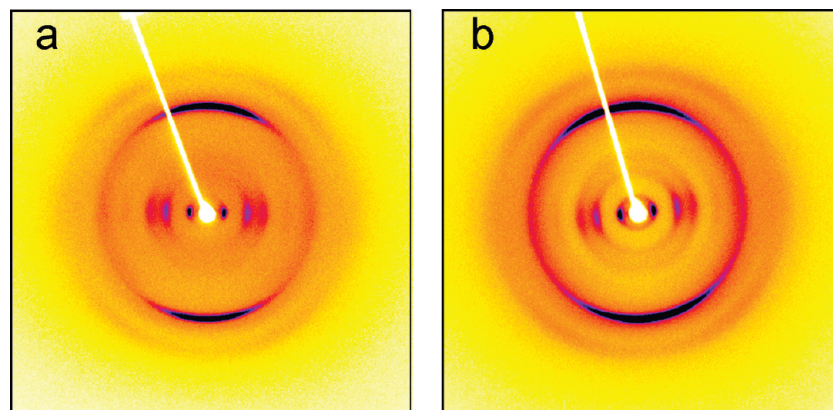


**Figure 1.** XRD patterns of dried stalks (a) YYKLVFFC, (b) YYKLVFFC with Congo red.

X-ray wavelength was  $\lambda = 1.54 \text{ \AA}$ . The wavenumber scale ( $q = 4\pi \sin \theta / \lambda$  where  $2\theta$  is the scattering angle) was geometrically calculated using the size of each pixel in the detector screen (0.0898 mm) and the sample–detector distance. The capillary flow cell was positioned with the flow direction  $\mathbf{v}$  parallel to the horizontal ( $x$ -axis) in the 2D detector plane.

**Linear Dichroism.** LD spectra were measured with a Couette cell inserted into the sample compartment of a J-815 spectropolarimeter (Jasco UK, Great Dunmow, U.K.) adapted for LD measurements. Solutions of YYKLVFFC (0.01 or 0.1 wt %) were loaded into a 60  $\mu\text{L}$  cylindrical quartz capillary of internal diameter 3 mm, one end of which is sealed with Araldite Rapide. A quartz rod of outer diameter 2.5 mm was suspended within the capillary and the capillary rotated within the Couette flow cell. This instrument is described in detail elsewhere.<sup>17</sup> The cell was built in-house; equivalent models are available from Kromatek (Great Dunmow, U.K.). Spectra were measured from 350 to 180 nm with a data point every 0.2 nm, scanning speed 100 nm/min, and a response time of 1 s. The bandwidth was 2 nm, and measurements were performed at room temperature. Spectra were measured at a cell rotation speed of 3000 rpm (equivalent to a shear rate  $\sim 1000 \text{ s}^{-1}$ ), and a nonrotating baseline spectrum was subtracted from each spectrum to account for the inherent LD signal of the system originating from the optics and the detector.

**Small-Angle X-ray Scattering.** SAXS data were collected on beamline ID02 at the ESRF, Grenoble, France. A 2 wt % YYKLVFFC sample in water (30  $\mu\text{L}$ ) was mounted in a flow-through capillary cell (diameter  $\sim 2$  mm). This cell provides lower background such that the sample and solvent scattering can be measured in the same position in the cell, allowing very reliable subtraction. For studies on the effect of reductant, mercaptoethanol (3  $\mu\text{L}$ ) was added to the YYKLVFFC solution, either by premixing and loading the mixed solution or by mixing inside the capillary (little difference was shown when comparing results under the two preparation conditions). SAXS data was collected using a FReLoN Kodak CCD detector. Sample–detector distances of 5 and 1.5 m were used. The X-ray wavelength was 0.995  $\text{\AA}$ .

**Near-Edge X-ray Absorption Fine Structure (NEXAFS) Spectroscopy.** NEXAFS experiments were performed on beamline I511-3 at MAX-lab, Lund, Sweden. A sample of YYKLVFFC was aligned by air-drying of a sample on a silicon substrate. Spectra of the aligned YYKLVFFC peptide were measured using a total fluorescence yield detector around the O, C, and N edges. The photon energy ranges used for these three regions are 525–550, 280–320, and 395–420 eV, respectively. Experiments were carried out first to study the grazing incidence

behavior (at normal incidence (NI) and 45°, 80° grazing incidence angles of the sample from the NI condition). The second aspect was the azimuthal angular dependency (at NI, changing the azimuthal angle of the sample). All the data presented in this report are the original data, normalized with respect to the beam current ( $I_0$ ), which was read on a photodiode.

## Results

**X-ray Diffraction and Raman Spectroscopy from Aligned Stalks.** X-ray diffraction (Figure 1) shows that well-aligned stalks can be prepared by drying YYKLVFFC solutions (1 wt %) using the method often used for amyloid peptides, drying of solutions between the wax-coated ends of two capillaries. We also performed XRD on a sample dried from a solution containing Congo red, since we were interested in investigating the possible binding of Congo red to the peptide, leading to potential structural modifications detectable by X-ray diffraction. SI Figure 1 confirms that YYKLVFFC is stained by Congo red, since apple-green birefringence is observed, which is diagnostic of amyloid formation. Figure 1 shows very little difference in the XRD pattern with and without Congo red. There is a difference in the extent of fibril orientation; however, this is usual due to variability in alignment from stalk to stalk. The sequence of observed equatorial and meridional reflections is the same with and without Congo red. Analysis of the cross- $\beta$  pattern for YYKLVFFC was discussed in our previous paper;<sup>4</sup> therefore, we conclude that XRD is unable to differentiate any structural effect upon binding of Congo red to YYKLVFFC. Lynn and co-workers also noted that Congo red has no effect on the cross- $\beta$  structure within nanotubes formed by the related peptide KLVFFAL.<sup>15</sup>

The orientational ordering of the fibrils in a stalk (without Congo red) was analyzed by X-ray diffraction measurements. The analytical solution<sup>27</sup> to Leadbetter's<sup>28,29</sup> expression for the analysis of X-ray diffraction from an ensemble of infinite rods with a distribution of orientation was solved numerically to obtain the values for the orientational order parameters  $\bar{P}_2$ ,  $\bar{P}_4$ , and  $\bar{P}_6$ . Order parameters  $\bar{P}_L$  are defined as

$$\bar{P}_L = \int_0^{\pi/2} P_L(\cos \beta) f(\beta) \sin \beta \, d\beta$$

Here,  $f(\beta)$  is the singlet orientational distribution function.

The intensity integrals were performed using the 4.75  $\text{\AA}$  meridional reflection. The calculation was performed at three different points of the stalk sample, and the results were averaged:  $\bar{P}_2 = 0.737 \pm 0.016$ ,  $\bar{P}_4 = 0.508 \pm 0.012$ ,  $\bar{P}_6 = 0.274$

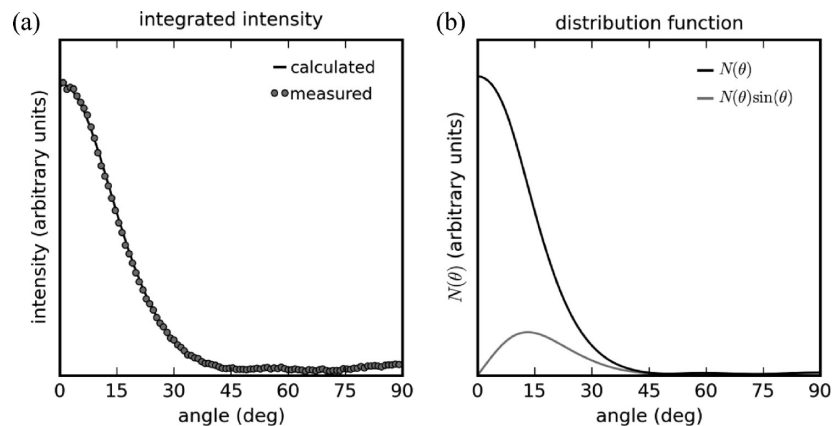


**Figure 2.** (a) Azimuthal variation of intensity of 4.8 Å main peak (averaged over four quadrants), points with fit (described in text) shown as a solid line. (b) Calculated orientational distribution function  $f(\beta)$  (black line) and weighted  $f(\beta) \sin \beta$  (gray line).

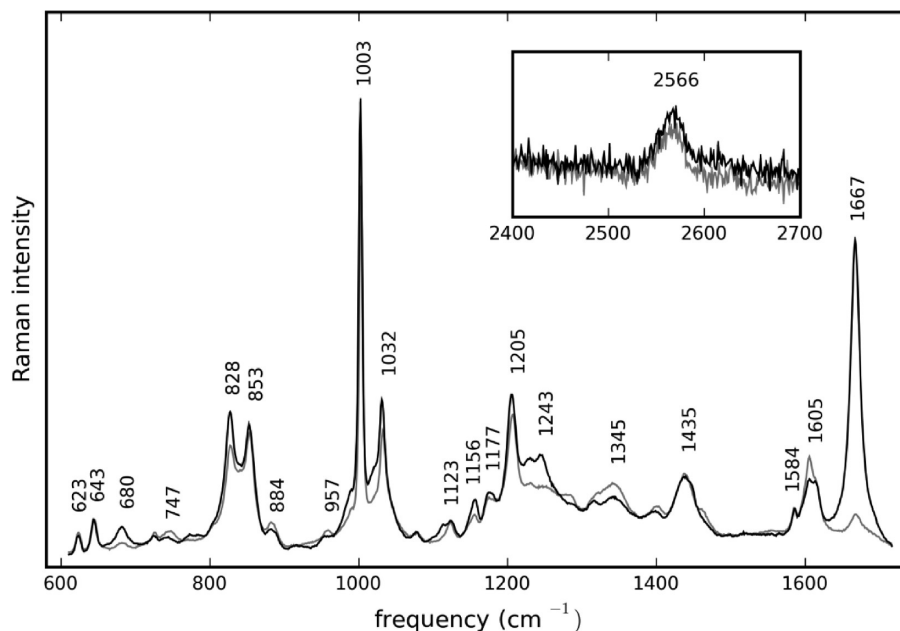


**Figure 3.** Polarized Raman spectrum from an aligned stalk, in the 600–1700  $\text{cm}^{-1}$  region. Black line:  $I_{cc}$ . Gray:  $I_{bb}$ . Inset: cysteine S–H stretch peak at 2566  $\text{cm}^{-1}$ .

$\pm 0:013$ . The small values for the standard deviation indicate a homogeneous alignment along the length of the stalk sample. The overall shape of the distribution of orientations of the fibrils,  $N(\theta)$  (Figure 2), which is obtained directly from the analysis of the azimuthal intensity variation in the X-ray diffraction data,<sup>27</sup> is determined by  $\bar{P}_2$  and  $\bar{P}_4$ . The obtained values denote a high degree of molecular alignment and a monotonic decrease in  $N(\theta)$  with the polar angle  $\theta$ .

Polarized Raman spectroscopy on an aligned stalk was used to gain insights into the self-assembled structure of YYKLVFFC fibrils. This technique has been used by others to obtain information about the orientation of molecular groups in a number of biological systems.<sup>30</sup> The results presented here provide some details about the conformation of the fibrils, although limited to a qualitative analysis. The polarized Raman spectra are presented in Figure 3. Peak assignments are summarized in Table 1. The notation for the spectra obtained with different configurations of the plane of polarization with respect to the fibril axis follow those introduced by Tsuboi.<sup>8</sup> In the following analysis, the cross-polarization spectra are neglected because they are weaker than the intensities  $I_{cc}$  (incident and scattered electric vectors parallel to direction of sample alignment) and  $I_{bb}$  (incident and scattered electric vectors

perpendicular to the director). In addition, pronounced dichroism of  $I_{cc}/I_{bb}$  is noted.

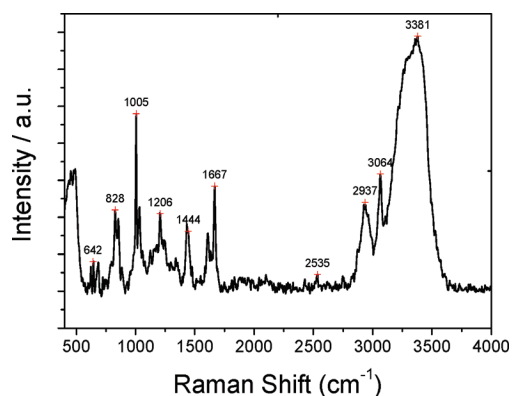
**Amide Backbone Vibrations.** In the polarized Raman spectrum of YYKLVFFC shown in Figure 3, the amide I band and the usual bands associated with aromatic side chains are the most prominent features of the spectrum. The position of the amide I peak, at 1667  $\text{cm}^{-1}$ , is normally assigned to antiparallel  $\beta$ -sheet structures.<sup>9</sup> This band shows a much greater intensity in the spectrum collected when both the incident and scattered light have their electric vectors polarized in the direction of sample alignment ( $I_{cc}$ ). The effective Raman tensor for antiparallel  $\beta$ -sheets has its maximum polarizability in the direction parallel to the carbonyl bonds.<sup>8</sup> The intensity of the amide I band is therefore consistent with a cross- $\beta$  structure, with the strands running perpendicular to the fibril axis. This observation is in agreement with the X-ray diffraction results performed on the same sample, showing the typical cross- $\beta$  pattern and a high degree of alignment (Figure 1).

**Cysteine-Related Features.** The spectroscopic signatures of S–S stretching bands appear in the vibrational spectra at about 500  $\text{cm}^{-1}$ .<sup>31–34</sup> The absence of signals in this region shows the absence of disulfide bonds in the dried stalks (a similar conclusion was reached from the Raman spectrum obtained for

**TABLE 1: Peak Assignments for the Raman Spectrum of YYKLVFFC Amyloid Fibrils<sup>a</sup>**

freq (cm <sup>-1</sup> )	assignment
2256	Cys S–H st
1667	amide I ( $\beta$ -sheets)
1613	Tyr (C <sub>2</sub> –C <sub>3</sub> and C <sub>5</sub> –C <sub>5</sub> in-phase st)
1605	Phe
1584	Phe
1435–1460	Leu, Val, Lys CH <sub>2</sub> , CH <sub>3</sub> bend
1345	C <sup><math>\alpha</math></sup> –H def
1230–1250	amide III
1205	Tyr C <sup><math>\beta</math></sup> –C <sup><math>\gamma</math></sup> , Phe
1177	Tyr C–H ring bend, F
1156	Val
1123	Leu, Val
1032	Phe
1003	Phe
957	Leu, C–C st
884	Lys, C–C and C <sup><math>\epsilon</math></sup> –C <sup><math>\zeta</math></sup> st
853	Tyr Fermi resonance doublet with 827, Phe
828	Tyr ring breathing vibration
747	Phe
680	Cys, C–S st
643	Tyr ring def
623	Phe

<sup>a</sup> Assignments were made on the basis of previous work by other authors on protein systems and model compounds.<sup>7,9,39,41,53,54</sup> St, stretching; def, deformation; bend, bending.

**Figure 4.** Raman spectrum for a 5 wt % solution in H<sub>2</sub>O.

a solution; vide infra). The peak observed at 2566 cm<sup>-1</sup>, from the cysteine S–H stretch, confirms this conclusion (Figure 4, inset). The frequency of the peak in the vibrational spectrum is correlated to the hydrogen bond strength of this moiety, with stronger hydrogen bonds shifted to lower wavenumbers.<sup>35</sup> On the basis of this correlation, it is concluded that the cysteine residue in YYKLVFFC is hydrogen bonded with a moderate strength.

The S–H stretching vibration also gives information about the presence of different hydrogen bonding environments within the polypeptide.<sup>36</sup> Although the signal-to-noise ratio in this region of the spectra is rather poor, it appears that a single peak is present. The cysteine residue is therefore participating in a hydrogen bond with a single acceptor and in a fixed geometry throughout the extent of the fibril. Peak area measurements reveal differences between the intensities  $I_{cc}$  and  $I_{bb}$  with only a marginally higher  $I_{cc}$  intensity (<5% difference), suggesting that both S–H bonds are not simultaneously aligned with respect to the fibril axis (either parallel or perpendicular) but are presumably tilted.

The peak at 680 cm<sup>-1</sup> is assigned to the C–S stretch vibration of cysteine.<sup>32</sup> Interestingly, this band has a greater intensity for

$I_{cc}$ . We do not have information about the specific shape of the Raman tensor for this vibration; however, being a stretching mode, it is expected to be cylindrical with its highest polarizability oscillation taking place along the axis of the bond. Polarized FTIR measurements on aligned YYKLVFFC amyloid fibrils suggest an antiparallel arrangement of the  $\beta$  sheets.<sup>37</sup> Thus, the higher intensity for  $I_{cc}$  indicates that the C <sup>$\beta$</sup> –S bond is preferentially aligned in a direction parallel to the fibril axis, making a hydrogen bond with one of the tyrosine residues from the next strand of the  $\beta$ -sheet.

**Tyrosine and Phenylalanine Features.** Aromatic amino acids give rise to the strongest bands in the Raman spectrum of proteins and peptides.<sup>38</sup> Not surprisingly, many of the assigned bands in the spectrum of YYKLVFFC have their origin in the phenylalanine and tyrosine residues (see Table 1 for assignments). Several of those bands show a different scattering intensity for the two spectra collected. Raman tensor values for several bands of tyrosine, which could be used to gain orientation information about these residues in YYKLVFFC, have been published.<sup>7</sup> However, a major problem resides in the overlapping of bands arising from both tyrosine and phenylalanine (for the latter of which there are no Raman tensors available), with the exception of the 828/853 cm<sup>-1</sup> tyrosine peaks. Furthermore, there are two instances of each amino acid in this system: all the peaks assigned to tyrosine and phenylalanine arise from at least two different residues. Considering these limitations, it is not possible to obtain quantitative information about the orientation of these side chains without making gross simplifications.

The significant dichroism of the 828 cm<sup>-1</sup> peak with higher signal parallel to the fibril alignment axis suggests that the ring normal is perpendicular to the fibril axis, as discussed in more detail below when results from Raman spectroscopy on dried stalks are compared with those from NEXAFS on surface-dried films. However, the assignment of this peak to tyrosine is ambiguous. For example, Overman et al. have assigned a peak at this position for a virus coat protein studied by them to phenylalanine.<sup>39,40</sup> They concluded that their spectra did not show the classical tyrosine Fermi doublet (828 + 850 cm<sup>-1</sup>). The 853 and 643 cm<sup>-1</sup> peaks in our spectrum do not show significant dichroism. The 1177 and 1205 cm<sup>-1</sup> peaks may be complicated by contributions from phenylalanine.<sup>40</sup>

**Fluorescence and Raman Spectroscopy Investigation of Dityrosine or Disulfide Cross-Linking.** As well as providing information on alignment and structure in dried stalks, Raman spectroscopy experiments were performed on solutions to examine the presence of  $\beta$ -sheet structure in solution. In addition, cysteine-related peaks were analyzed to investigate possible oxidative disulfide cross-linking of the peptide. Raman spectroscopy was performed using a 5 wt % solution in H<sub>2</sub>O. As discussed for the dried stalk Raman data, on the basis of previous reports,<sup>31–33,35</sup> a peak from S–H (i.e. uncross-linked thiol units) is expected at 2525–2580 cm<sup>-1</sup> (peak positions calculated for model compounds are higher than those measured). A peak within this range, at 2535 cm<sup>-1</sup>, is observed, as shown in Figure 4. As mentioned above, the position of this peak relates to hydrogen bond strength, and a peak at 2535 cm<sup>-1</sup> indicates strong hydrogen bonding of the S–H donors.<sup>35</sup>

In contrast, a peak associated with disulfide S–S stretch deformations, observed,<sup>34</sup> for example, for the protein *Escherichia coli* thioredoxin at 507 cm<sup>-1</sup> or other proteins or model peptides at 506–514 cm<sup>-1</sup><sup>33</sup> is absent. These results indicate that free thiol groups are present in the cysteine units of YYKLVFFC, that these are strongly hydrogen bonded to H<sub>2</sub>O,

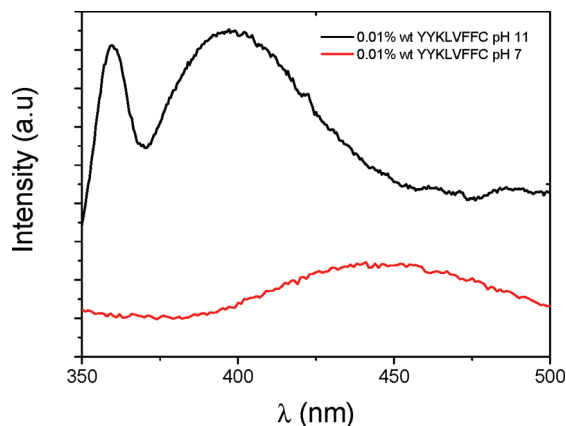


Figure 5. Fluorescence emission spectrum ( $\lambda_{\text{ex}} = 320$  nm).

and that there is no evidence for disulfide bridging under native pH conditions. These spectra also provide evidence for unasociated tyrosine residues, in particular, the peaks at 1206, 828/853, and 642  $\text{cm}^{-1}$  can be assigned to Y residues (subject to certain provisos, discussed above).

These peaks are in a location very similar to the corresponding peaks for the dried stalk (Table 1). The pair of peaks at 1004  $\text{cm}^{-1}$  and 1035  $\text{cm}^{-1}$  are assigned to F residues (cf. Table 1).<sup>9,34,38,41</sup> The peak at 1444  $\text{cm}^{-1}$  can be assigned to a C–H bend deformation.<sup>9,34</sup> Features in the amide I region at 1667  $\text{cm}^{-1}$  are prominent and indicate  $\beta$ -sheet formation. As mentioned above, the latter peak as also observed for the dried stalk is usually associated with antiparallel  $\beta$ -sheet formation, which was also confirmed by polarized FTIR spectroscopy and will be reported elsewhere.<sup>37</sup> There are also strong peaks above 2900  $\text{cm}^{-1}$ , assigned to C–H stretch deformations.<sup>34</sup>

Further evidence for the absence of disulfide cross-linking was provided by mass spectrometry, since there was no evidence for ions with molecular weights above those of the peptide itself (SI Figures 2–4).

Fluorescence spectroscopy was performed to investigate possible dityrosine formation under alkaline conditions. Figure 5 shows the emission spectrum obtained for  $\lambda_{\text{ex}} = 320$  nm. It shows a peak at  $\sim 400$  nm (the peak at 360 nm is associated with Raman scattering from water).<sup>42</sup> A peak close to 400 nm is associated with dityrosine formation.<sup>43,44</sup> This peak is absent at pH 7, as expected, since the tyrosine hydroxyl unit is present in phenol form under these conditions, rather than the phenolate form at alkaline pH. The excitation spectra (Figure 6) show a red-shift of the 305 nm peak on increasing pH, with an increase in intensity. The position of the peak in the excitation spectrum is also consistent with dityrosine formation at pH 11.<sup>44</sup> In the following studies of alignment on solutions, we therefore avoid alkaline pH conditions in which dityrosine links may exist. Similarly, in the preparation of stalks and films for polarized Raman and NEXAFS samples, respectively, alkaline pH conditions were avoided.

**Linear Dichroism and SAXS/WAXS on Flow Aligning Solutions.** UV/visible linear dichroism provides information on the orientation of subunits (transition dipoles associated with particular bonds) in a molecule with respect to an alignment direction. The LD spectrum of YYKLVFFC was obtained for a sample aligned by flow in a Couette cell. Spectra were recorded during the process of self-assembly (measurements every 30 min) after dissolving the peptide in water under native pH conditions (time  $t = 0$ ). The measured spectra are shown in Figure 7.

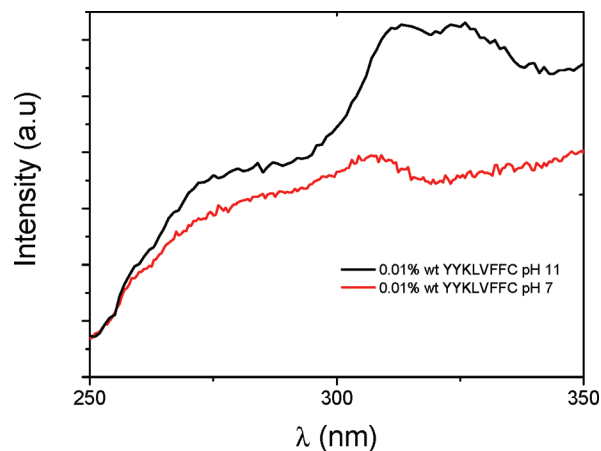


Figure 6. Fluorescence excitation spectrum (emission monitored at 410 nm).

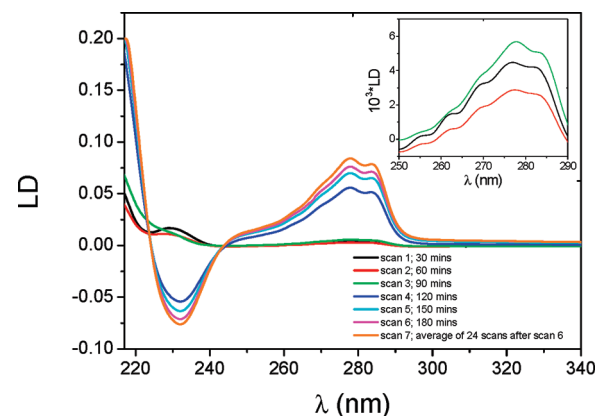


Figure 7. Linear dichroism spectra measured after dissolution of YYKLVFFC in water. Spectra were recorded every 30 min to monitor the self-assembly process. The inset shows enlarged spectra after 30, 60, and 90 min in the 250–290 nm wavelength range, showing fine structure from the F residues.

The sign of the linear dichroism,

$$\text{LD} = A_{\parallel} - A_{\perp}$$

in the spectrum (where  $A_{\parallel}$  and  $A_{\perp}$  are absorbances parallel and perpendicular to the flow direction, respectively), provides information on the alignment of the backbone and aromatic units in YYKLVFFC. The  $\pi$ – $\pi^*$  transition arising from the carbonyl bonds in the peptide backbone gives rise to a peak at 195 nm.<sup>15,16,18</sup> Longer wavelength bands are attributed to the peptide  $n$ – $\pi^*$  transition at about 220 nm and tyrosine transitions at 280 and 230 nm. The phenylalanine peaks are centered around 260 nm.

The spectra in Figure 7 show increasing and positive LD as wavelength decreases (data obtained at lower wavelength were truncated due to saturation of absorbance). The fact that the LD is positive in the low wavelength region indicates that the C = O bonds are parallel to the alignment (fibril direction); that is, the peptide backbone is perpendicular to the fibril direction,<sup>18,19,45</sup> as is usual in a cross- $\beta$  amyloid structure. The LD at low wavelength increases during the process of YYKLVFFC fibrillization showing fibril formation with  $\beta$  strands perpendicular to the fibril axis.

The near-UV region of the spectrum is dominated by contributions from the aromatic residues tyrosine and phenylalanine due to their high extinction coefficients.<sup>46</sup> The strongest

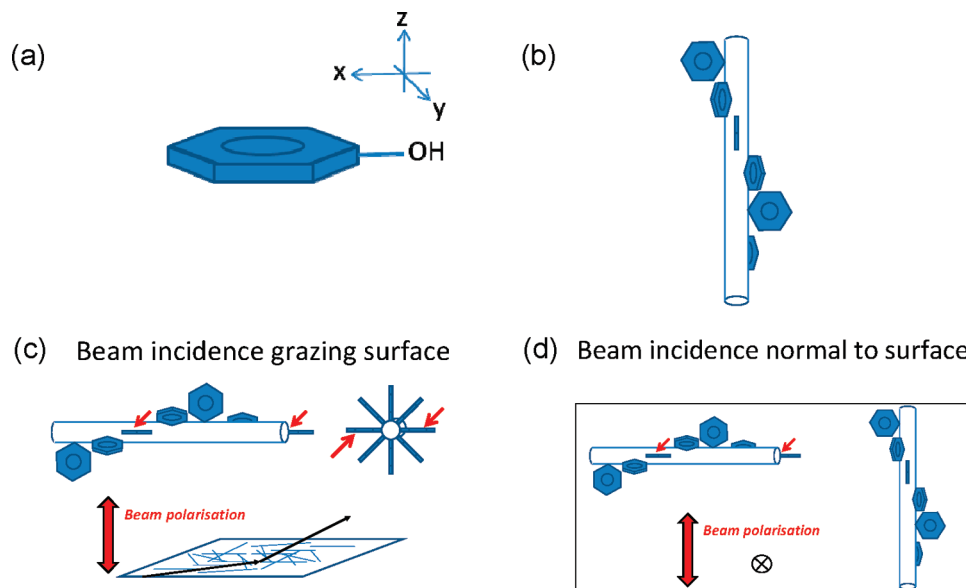


**Figure 8.** Tyrosine alignment from Raman spectroscopy, LD and NEXAFS. (a) Definition of local axis system; (b) schematic of rings with normals orthogonal to fibril axis as deduced from LD on a flow-aligned solution, and Raman spectroscopy on a stalk; (c) grazing incidence NEXAFS configuration; and (d) normal incidence NEXAFS configuration.

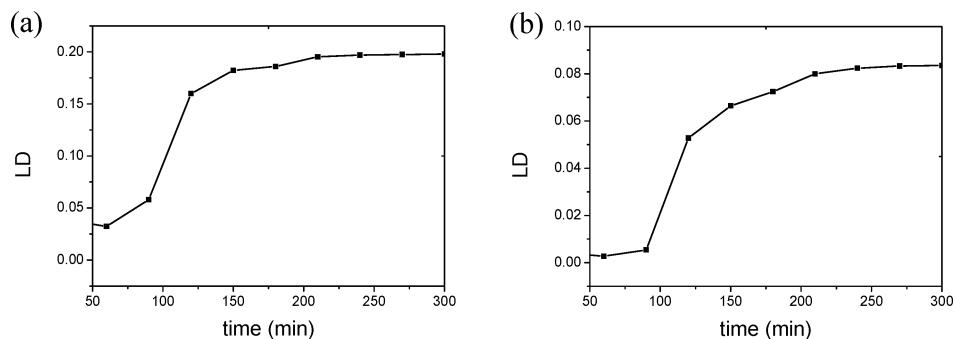


**Figure 9.** Kinetics of self-assembly monitored for a 0.01 wt % solution of YYKLVFFC by time-dependent LD at (a) 218 and (b) 280 nm.

feature is the doublet at 278 and 283 nm, which is due to the tyrosine residues.<sup>18,19,45</sup> There are also small peaks between 250 and 280 nm arising from the vibrational modes of phenylalanine that can arise only if the phenylalanine side chain is ordered and, hence, well-aligned in the fiber. The inset in Figure 7 shows fine structure resulting from absorption features of this chromophore (expected extinction coefficient maxima are at 263, 257, and 252 nm).<sup>46,48</sup> The fact that these features are observed during the initial stages of the self-assembly process points to a regular packing of phenylalanine residues at an early stage. This is consistent with our hypothesis for related peptide fragments that phenylalanine packing driven by aromatic stacking interactions drives the initial self-assembly.<sup>5</sup> The phenylalanine features get washed out when the strong peaks from tyrosine residues develop as fibrillization progresses.

In the spectra at the start of the time course, the two tyrosine peaks at 278 and 283 nm are shifted about 3 nm higher in wavelength from the position that would be expected for an aqueous environment.<sup>49</sup> This suggests that the tyrosines are sequestered in the fiber, away from the bulk solvent or that the excited state is stabilized by  $\pi$ -stacking of the aromatic side chains, or both. There is a further 2 nm shift as the fibers mature over the next few hours. The transition dipole for the tyrosine absorbance around 280 nm ( $L_b$ ) lies perpendicular to the C–O bond (along  $y$  in Figure 8a), and the dipole for the tyrosine absorbance around 230 nm ( $L_a$ ) lies along  $x$  in Figure 8a. At the start of the time course, there is a positive signal at 230 and

280 nm: this can arise only if both transition dipoles are at  $<54.7^\circ$  from the fiber long axis. At later times, the signals at 230 and 280 nm are negative and positive, respectively. This means that the  $L_a$  and  $L_b$  transition dipoles are pointing, respectively, perpendicular and parallel to the fiber long axis, as illustrated in Figure 8b.

At early time points, there is a significant LD signal that increases dramatically after 2 h. This is caused by the fibers becoming more aligned as a result of being longer or stiffer. This is further quantified in Figure 9, which shows the time-dependence of the LD at certain fixed wavelengths associated with backbone and tyrosine transitions. Rapid growth in the LD occurs between 90 and 120 min, correlated to fibrillization, and following on from an initial incubation (nucleation) period, the curves exhibiting a similar sigmoidal shape. The spectra in the near UV region are flat and independent of time. This points to the absence of light-scattering effects, possibly because the fibrils of YYKLVFFC are not very elongated,<sup>4</sup> in contrast to previous work on Sup35 amyloid fragment GNNQQNY, for which the intensity in the 300–340 nm region increased with time due to fibrillization and crystallization.<sup>47</sup>

The reduced LD at a particular wavelength,  $LD^r$  is related to the orientation of the subunit giving rise to the signal at that wavelength by the following relationship:<sup>16,47</sup>

$$LD^r = LD/A = \frac{3}{2}\bar{P}_2(3 \cos^2 \alpha - 1)$$

Here,  $A$  is the isotropic absorbance,  $\alpha$  is the angle between the alignment axis and the transition dipole giving rise to the LD at a reference wavelength, and  $\bar{P}_2$  is the orientational order parameter. This relationship enables information on the angle of orientation of tyrosine residues to be obtained, knowing the orientational order parameter or vice versa. Since YYKLVFFC contains two tyrosine residues and contributions from these cannot be separated in the spectrum, this analysis is prohibited unless it is assumed that both have a similar orientation. Furthermore, the order parameter,  $\bar{P}_2$ , is not known in solution (we report values above from XRD on a dried stalk). In principle, it should be possible to obtain  $\bar{P}_2$  from the LD  $\pi$ - $\pi^*$  backbone signal (for which  $\alpha = 90^\circ$  is known); however, the absorbance was saturated at low wavelength, as mentioned above.

LD with continuous pumped flow (sample in a flat quartz cell) has been used to probe the alignment of an amyloid-forming fragment of  $\beta$ -microglobulin.<sup>19</sup> The LD associated with the  $\pi$ - $\pi^*$  transition moment of the carbonyl group indicated alignment of the carbonyl group parallel to the fibril axis. The LD associated with the  $L_b$  transition of tyrosine indicated that this transition moment was also aligned along the fibril axis; that is, the tyrosine phenyl ring normal was perpendicular to both the peptide backbone and the fibril axis.<sup>19</sup> Our results for YYKLVFFC show similar features. The same technique has also been used to examine the alignment of nanotubes formed by peptide KLVFFAL, which contains the same KLVFF motif as YYKLVFFC.<sup>15</sup> The observed positive LD indicated that the carbonyl bonds were aligned roughly parallel to the nanotube axis, pointing toward strands perpendicular to the axis of the self-assembled superstructure.

SAXS confirms spontaneous alignment of YYKLVFF upon flow into a capillary. This resulted from the sample loading procedure and as such was not a controlled capillary flow experiment. SI Figure 5 shows SAXS patterns obtained for 2 wt % solutions of YYKLVFFC in water (native pH) with and without mercaptoethanol. There is no qualitative difference in the SAXS patterns (and almost no quantitative difference in the cross sections shown in SI Figure 5, part c), and therefore, mercaptoethanol seems not to influence the fibrillar superstructure or extent of alignment. This supports our findings from Raman spectroscopy, discussed above, concerning the absence of disulfide formation under native pH conditions.

SAXS data for a 1 wt % sample of YYKLVFFC also showed strong alignment. The anisotropic SAXS pattern was analyzed in detail in our previous paper.<sup>4</sup> We obtained a fibril radius of 18.4 Å, and a lower limit of fibril length of 1000 nm; that is, effectively infinite considering the  $q$  range of the experiment. The data in SI Figure 5 for the 2 wt % solutions of YYKLVFFC show the development of a structure factor peak that was not present for the 1 wt % solutions, which could be analyzed solely on the basis of form factor. The structure factor maximum at  $q = (0.0240 \pm 0.0002) \text{ \AA}^{-1}$  points to an average spacing between flow aligning fibrils of  $(261 \pm 3) \text{ \AA}$ , which is substantially larger than the fibril radius, pointing to a low packing density of fibrils.

The onset of nematic ordering from the Onsager criterion is expected to occur at a volume fraction  $\phi_c = 4.5D/L$  which can be evaluated, using the lower bound for the fibril length  $L$  mentioned above, to be  $\phi_c = 0.017$ , corresponding to  $\sim 1.7$  wt % sample. We find that the experimental boundary lies slightly lower, between 0.5 wt % peptide and 1 wt % peptide. Mezzenga

et al. have noted that for  $\beta$ -lactoglobulin, the Onsager theory overestimates the I-N transition temperature by an order of magnitude as compared with the measured value.<sup>50</sup> This difference was not resolved by considering the semiflexible and charged nature of the fibrils. They were able to account for this discrepancy by invoking Flory's theory for the I-N phase transition arising from unfavorable rod/solvent interactions in solution. However, this level of quantitative modeling is not justified in our present study.

Separate XRD experiments were performed on samples under controlled capillary flow conditions. For each sample, the flow behavior was studied for flow rates in the range  $Q = (0.1-6) \text{ mL min}^{-1}$  at room temperature. The general features of the XRD patterns for 1 and 2 wt % YYKLVFFC did not change as a function of the flow rate within the range  $Q = (0.1-6) \text{ mL min}^{-1}$ . Figure 10a and b shows the XRD patterns obtained for 1 and 2 wt % solutions of YYKLVFFC, respectively. The XRD data is characterized by two weak oscillations centered at  $q = 0.3017$  and  $0.6131 \text{ \AA}^{-1}$  and a sharp reflection centered at  $q = 1.3212 \text{ \AA}^{-1}$ . The XRD patterns in Figure 10 remain unchanged 60 min after stopping the shear flow. The presence of these reflections confirms that the cross- $\beta$  structure is retained in solution under flow.<sup>51</sup>

Figure 11 contains the radial averages of the patterns in Figure 10. The sharp reflection at  $q = 1.3212 \text{ \AA}^{-1}$  corresponds to a spacing  $d = 4.75 \text{ \AA}$ , from the separation between peptide backbones within the  $\beta$ -sheet. The peaks at  $q = 0.3017 \text{ \AA}^{-1}$  ( $d = 21 \text{ \AA}$ ) and  $0.6131 \text{ \AA}^{-1}$  ( $d = 10.2 \text{ \AA}$ ) are associated with the stacking of the  $\beta$ -sheets, although the positions differ from those observed for dried stalks, reflecting a dehydration effect. The intensities of the peaks are enhanced upon increasing concentration. The azimuthal profiles of the patterns in Figure 10 (not shown) confirm that the equatorial arc centered at  $4.75 \text{ \AA}$  remains oriented at  $\sim 180^\circ$  and keeps an angular width of  $\sim 30^\circ$ . These conditions proved to be valid for the whole shear range  $Q = (0.1-6) \text{ mL min}^{-1}$  and up to 60 min after the shear was stopped.

**NEXAFS.** Polarized NEXAFS spectroscopy was used to investigate the alignment of specific bonds within a film of YYKLVFF dried onto a silicon substrate. In the O-NEXAFS region, the  $\pi$ -resonance peak due to the carbonyl system appears at 531.4 eV, accompanied by broad sigma resonance at 538.7 eV. The highest intensity was observed at  $80^\circ$  grazing incidence, which indicates that the carbonyl group lies almost flat on the surface. (Figure 12a).

In the C-NEXAFS region (Figure 12b), two sharp peaks, 284.9 and 287.8 eV, are observed that belong to two  $\pi$ -resonance systems in the peptide structure, phenyl ring and the carbonyl group, respectively. The broad sigma resonances, 291.3 and 298.3 eV, due to single bonds (C-C, C-N, etc.) follow the  $\pi$ -resonance peaks. Changing the grazing incidence angle of the sample, small variations in the intensities of peaks were observed, indicating an angular dependency. Both  $\pi$ -resonances show the same type of angular dependency, indicating that carbonyl and phenyl  $\pi$ -systems lie in the same plane. From O-NEXAFS, it has thus been concluded that the carbonyl group is almost flat on the surface, so the phenyl ring should also lie preferentially parallel to the surface.

In the N-NEXAFS region (Figure 12c), three small  $\pi$ -resonance peaks (398.2, 399.3, 400.8 eV) are observed. These peaks were observed previously for self-assembling peptides, including EAK16 (H-AKAKAEAEAKAKAEAE-NH<sub>2</sub>)<sup>52</sup> and related derivatives deposited on on TiO<sub>2</sub>.<sup>12-14</sup> In these reports, the first two peaks are reported to be significantly smaller as compared



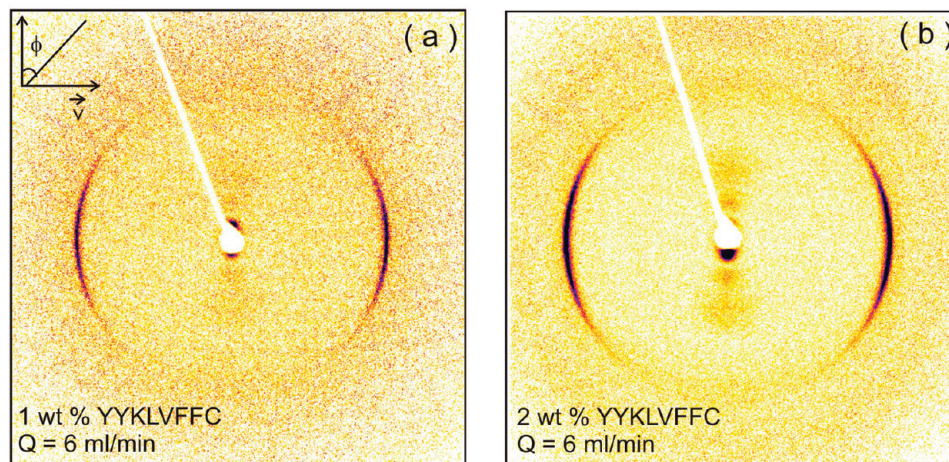


**Figure 10.** XRD obtained for (a) 1 and (b) 2 wt % YYKLVFFC. The inset shows the azimuthal coordinates and the flow direction with respect to the 2D image on the detector. All the data have been obtained at  $Q = 6 \text{ mL min}^{-1}$ .

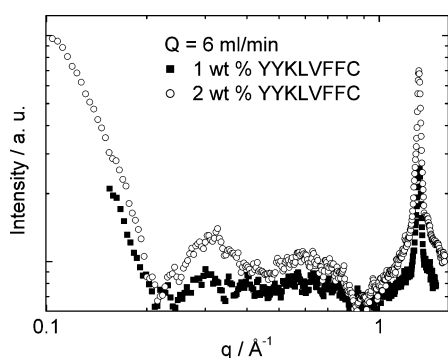


**Figure 11.** Radial intensity obtained from the XRD patterns displayed in Figure 11.

with the main  $\pi$  resonance peak at 402 eV. The main peak may be due to the resonance structure taking place due to the relocation of the nitrogen free electrons on the carbonyl group. However, the observation of a lower intensity for the main peak at 400.8 eV for YYKLVFFC could mean a hindered or trapped electron, creating an inequality in this resonance system. Again, the maximum intensity is observed at  $80^\circ$  grazing incidence, indicating that the N-resonance is also almost parallel to the surface.

In addition to the above experiments, the azimuthal angular dependency of NEXAFS spectra was examined (data not shown). Very little if any anisotropy was noted, indicating that the peptide fibrils do not have preferential orientation within the plane of the film.

**Comparison of Alignment: Raman on Stalk vs NEXAFS on Film.** The O-NEXAFS spectrum shows that the peptide C=O bonds and, therefore, the fibril axis are oriented, on average, parallel to the surface. The C-NEXAFS peak at 285 eV shows a slight angular dependence, suggesting that, on average, the phenyl rings (present, unfortunately, on both YY and FF) are also oriented parallel to the surface. More specifically, a signal is obtained when the NEXAFS beam polarization is perpendicular to the phenyl ring, and this is greater with a grazing incidence beam than one normal to the surface. So it can be deduced that more phenyl rings have their normal perpendicular to the surface than in either one of the directions parallel to the surface.

We now consider the information from the Raman spectra obtained for a different uniaxial system (dried stalk), with *positive* orientational order parameters (as determined from

XRD). As mentioned above (i) the amide I band shows very high orientation of CO bonds parallel to fibril axis, consistent with cross- $\beta$  structure and NEXAFS results, and (ii) the tyrosine in-plane ring stretch band at  $828 \text{ cm}^{-1}$  clearly shows dichroism with higher signal parallel to the fibril alignment axis. Because the Raman tensor has  $r_1 = \alpha_{xx}/\alpha_{zz} = 2.2$  and  $r_2 = \alpha_{yy}/\alpha_{zz} = 2.0$ , this gives a bigger signal if either of the in-plane  $x$ - or  $y$ -axes (Figure 8a) are aligned with the polarization, and a smaller signal if the polarization is aligned with the  $z$ -axis (normal to the plane of the ring). Thus, the dichroism here suggests that the ring normal ( $z$ -axis) is perpendicular to the fibril axis. Whether this means that the fibrils are parallel to the  $x$ - or  $y$ -direction cannot be determined. Assuming that the fibril has uniaxial symmetry, the tyrosine phenyl ring will be arranged as shown schematically in Figure 8b.

Going back to the NEXAFS data, assuming uniaxial cylindrical symmetry about the fibril axis and then distributing the fibrils within the plane of the surface, it is possible to deduce that there will be more aromatic rings with normals parallel to the polarization of the NEXAFS beam when the NEXAFS beam is at grazing incidence. Referring to Figure 8c,d: In each case, the beam is going into the page, and its polarization is vertical. In Figure 8c, the beam is grazing the surface (which is horizontal, going into the page). Assuming that all of the fibrils are in the plane of the surface, some are also in the plane of the page, and some are going into the page. All fibrils will have some phenyl rings (marked with diagonal red arrows) with normals aligned with the polarization and, therefore, that can give a signal. On the other hand, when the beam is incident normal to the surface (Figure 8d), then fibrils where the axis is itself aligned with the beam polarization (such as the one on the right) will not have phenyl rings aligned in the correct fashion. Thus, using the information on phenyl group orientation with respect to the fibril axis from the Raman spectrum, it is possible to show that the NEXAFS data indicate that in films, phenyl rings preferentially have their normal perpendicular to the surface.

## Summary

The combination of methods applied yields unprecedented insight into the alignment of beta strands and aromatic side chains within a model amyloid peptide, YYKLVFFC. Polarized Raman spectroscopy on a dried stalk indicates that tyrosine phenyl ring normals are perpendicular to the fibril axis; that the  $\beta$ -strands are perpendicular to the fibril axis, as in a usual

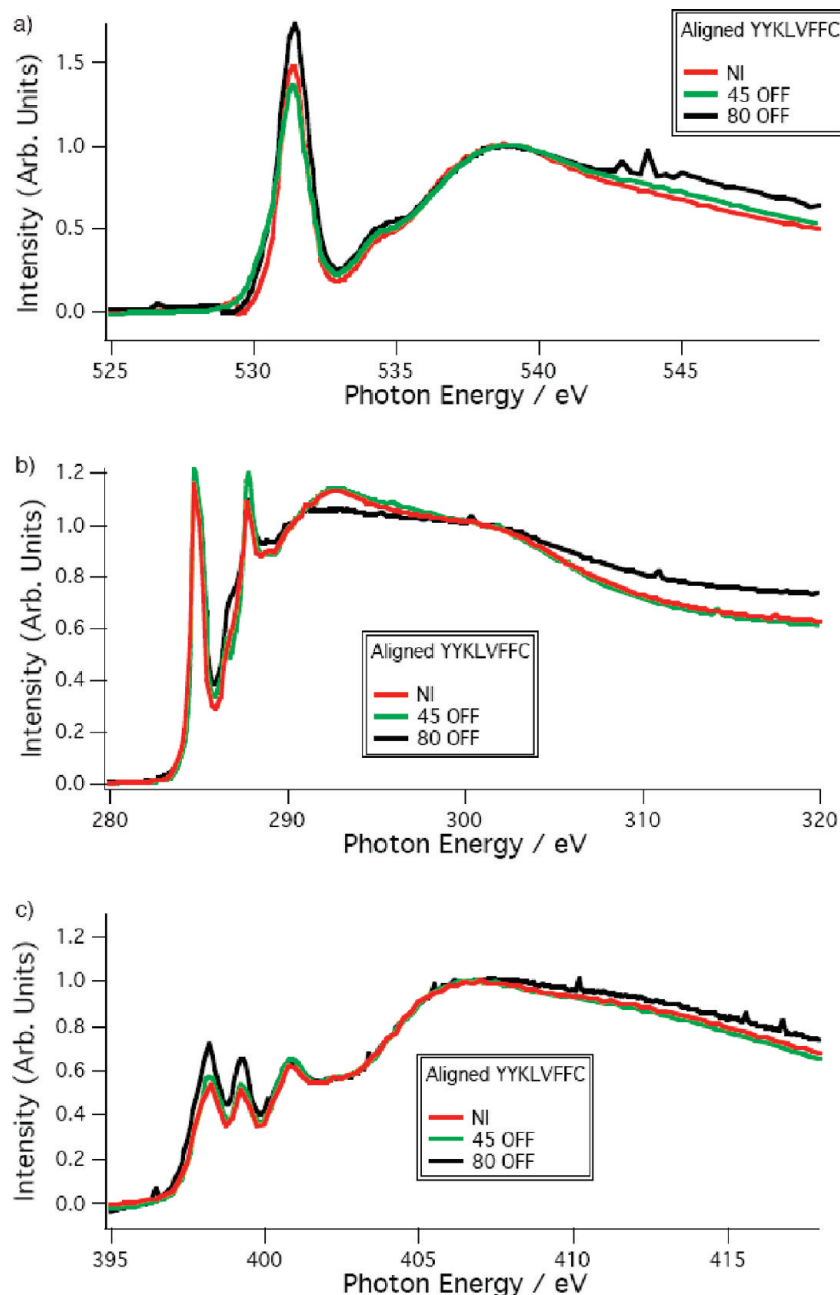


**Figure 12.** (a) O-NEXAFS, (b) C-NEXAFS, and (c) N-NEXAFS spectra of YYKLVFFC under different grazing incidence angle conditions.

cross- $\beta$  structure; and that free S-H is present (and that this bond is tilted), showing the absence of disulfide formation. X-ray diffraction on the same dried stalk provided orientational order parameters and the singlet orientational distribution function by analyzing the azimuthal dependence of the intensity of the 4.8 Å reflection from the backbone spacing. X-ray diffraction also indicated that binding of Congo red does not change the structure of the fibrils at the level of the cross- $\beta$  pattern.

In solution, Raman spectroscopy likewise confirmed the presence of  $\beta$ -sheet structure and the absence of disulfide bond formation. Fluorescence spectroscopy was used to examine dityrosine formation. This was observed under alkaline conditions, but not at neutral pH, as expected. LD provided information both on the mechanism and kinetics of self-assembly in a solution subjected to flow alignment and on the orientation of strands and aromatic units that complements polarized Raman spectroscopy performed on dried stalks. LD shows that the carbonyl units are aligned along the fibril axis and that tyrosine

units are aligned with the C=O bond perpendicular to the fibril axis (phenyl rings “edge on”). Peaks arising from phenylalanine are present in the early stages of fibrillization, pointing to an initial self-assembly process driven by these highly hydrophobic aromatic residues. There is a nucleation stage, followed by rapid fibrillization between 90 and 120 min after dissolution of the peptide. The tyrosine features in the near UV spectrum become dominant over phenylalanine contributions over this interval. X-ray diffraction on a solution subjected to shear confirms retention of cross- $\beta$  structure and alignment along the flow direction. SAXS shows orientation of fibrils at a larger length scale.

NEXAFS was used to probe alignment at the surface of dried films on silicon and indicates C=O bonds parallel to the surface and a predominance of phenyl rings with normals perpendicular to the surface. These techniques have great potential to be developed to further quantify the orientation of specific subunits. This would be facilitated by the design of peptides with only

single tyrosine or phenylalanine units (or both) and thus will be the subject of future work.

**Acknowledgment.** This work was supported by EPSRC grants EP/F048114/1 and EP/G026203/1 to I.W.H. We thank MaxLab (Lund, Sweden) for the award of NEXAFS beamtime (ref 511/3-261) and Franz Hennies (Beamline scientist) and Anders Olsson (Beamline Engineer) for their support. The research leading to the results at MaxLab has received funding from the European Community's Seventh Framework Programme (FP7/2007-2013) under Grant agreement no. 226716. We are grateful to researchers in the Biocentre (University of Reading) for help with XRD (Nick Spencer) and mass spectroscopy (Trevor Gibson and Davinia Mills).

**Supporting Information Available:** Additional information as noted in text. This material is available free of charge via the Internet at <http://pubs.acs.org>.

## References and Notes

- Mata, A.; Hsu, L.; Capito, R.; Aparicio, C.; Henrikson, K.; Stupp, S. I. *Soft Matter* **2009**, *5*, 1228–1236.
- Marklein, R. A.; Burdick, J. A. *Adv. Mater.* **2010**, *22*, 175–189.
- Gras, S. L.; Tickler, A. K.; Squires, A. M.; Devlin, G. L.; Horton, M. A.; Dobson, C. M.; MacPhee, C. *Biomaterials* **2008**, *29* (11), 1553–1562.
- Hamley, I. W.; Castelletto, V.; Moulton, C. M.; Myatt, D.; Siligardi, G.; Oliveira, C. L. P.; Pedersen, J. S.; Gavish, I.; Danino, D. *Macromol. Biosci.* **2010**, *10*, 40–48.
- Krysmann, M. J.; Castelletto, V.; Kelarakis, A.; Hamley, I. W.; Hule, R. A.; Pochan, D. J. *Biochemistry* **2008**, *47*, 4597–4605.
- Ban, H.; Gavriluk, J.; Barbas, C. F. *J. Am. Chem. Soc.* **2010**, *132*, 1523–1525.
- Tsuboi, M.; Ezaki, Y.; Aida, M.; Suzuki, M.; Yimit, A.; Ushizawa, K.; Ueda, T. *Biospectroscopy* **1998**, *4* (1), 61–71.
- Tsuboi, M.; Kubo, Y.; Akahane, K.; Benevides, J. M.; Thomas, G. J. *J. Raman Spectrosc.* **2006**, *37* (1–3), 240–247.
- Rousseau, M. E.; Lefevre, T.; Beaulieu, L.; Asakura, T.; Pezolet, M. *Biomacromolecules* **2004**, *5* (6), 2247–2257.
- Tsuboi, M.; Kubo, Y.; Ikeda, T.; Overman, S. A.; Osman, O.; Thomas, G. J. *Biochemistry* **2003**, *42* (4), 940–950.
- Overman, S. A.; Tsuboi, M.; Thomas, G. J. *Biophys. J.* **1998**, *74* (2), A73–A73.
- Polzonetti, G.; Battocchio, C.; Lucci, G.; Dettin, M.; Gambaretto, R.; Di Bello, C.; Carravetta, V. *Mater. Sci. Eng., C* **2006**, *26* (5–7), 929–934.
- Lucci, G.; Battocchio, C.; Dettin, M.; Gambaretto, R.; Di Bello, C.; Borgatti, F.; Carravetta, V.; Monti, S.; Polzonetti, G. *Surf. Sci.* **2007**, *601* (18), 3843–3849.
- Lucci, G.; Battocchio, C.; Dettin, M.; Gambaretto, R.; Polzonetti, G. *Surf. Interface Anal.* **2008**, *40* (3–4), 210–214.
- Childers, W. S.; Mehta, A. K.; Lu, K.; Lynn, D. G. *J. Am. Chem. Soc.* **2009**, *131* (29), 10165–10172.
- Bulheller, B. M.; Rodger, A.; Hirst, J. D. *Phys. Chem. Chem. Phys.* **2007**, *9* (17), 2020–2035.
- Marrington, R.; Dafforn, T. R.; Halsall, D. J.; Rodger, A. *Biophys. J.* **2004**, *87* (3), 2002–2012.
- Rodger, A.; Marrington, R.; Geeves, M. A.; Hicks, M.; de Alwis, L.; Halsall, D. J.; Dafforn, T. R. *Phys. Chem. Chem. Phys.* **2006**, *8* (27), 3161–3171.
- Adachi, R.; Yamaguchi, K.; Yagi, H.; Sakurai, K.; Naiki, H.; Goto, Y. *J. Biol. Chem.* **2007**, *282* (12), 8978–8983.
- Hiramatsu, H.; Goto, Y.; Naiki, H.; Kitagawa, T. *J. Am. Chem. Soc.* **2004**, *126* (10), 3008–3009.
- Hiramatsu, H.; Kitagawa, T. *Biochim. Biophys. Acta* **2005**, *1753*, 100–107.
- Kim, H. S.; Hartgerink, J. D.; Ghadiri, M. R. *J. Am. Chem. Soc.* **1998**, *120*, 4417–4424.
- Paramonov, S. E.; Jun, H.-W.; Hartgerink, J. D. *J. Am. Chem. Soc.* **2006**, *128*, 7291–7298.
- Castelletto, V.; Hamley, I. W.; Harris, P. J. F. *Biophys. Chem.* **2008**, *139*, 29–35.
- Krysmann, M. J.; Castelletto, V.; Hamley, I. W. *Soft Matter* **2007**, *3*, 1401–1406.
- Castelletto, V.; Hamley, I. W. *Polym. Adv. Technol.* **2006**, *17* (3), 137–144.
- Deutsch, M. *Phys. Rev. A* **1991**, *44* (12), 8264–8270.
- Leadbetter, A. J.; Norris, E. K. *Mol. Phys.* **1979**, *38* (3), 669–686.
- Leadbetter, A. J., Structural studies of nematic, smectic A and smectic C phases. In *The Molecular Physics of Liquid Crystals*; Luckhurst, G. R., Gray, G. W., Eds.; Academic: London, 1979; pp 286–316.
- Tsuboi, M.; Benevides, J. M.; Thomas, G. J. *Proc. Jpn. Acad., Ser. B* **2009**, *85* (3), 83–97.
- Sugeta, H.; Go, A.; Miyazawa, T. *Chem. Lett.* **1972**, 82–86.
- Wart, H. E. V.; Lewis, A.; Scheraga, H. A.; Saeva, F. D. *Proc. Natl. Acad. Sci. U.S.A.* **1973**, *70* (9), 2619–2623.
- Qian, W.; Zhao, W.; Krimm, S. *J. Mol. Struct.* **1991**, *250*, 89–102.
- Li, H.; Hanson, C.; Fuchs, J. A.; Woodward, C.; Thomas, G. J. *Biochemistry* **1993**, *32*, 5800–5808.
- Li, H. M.; Thomas, G. J. *J. Am. Chem. Soc.* **1991**, *113* (2), 456–462.
- Raso, S. W.; Clark, P. L.; Haase-Pettingell, C.; King, J.; Thomas, G. J. *J. Mol. Biol.* **2001**, *307* (3), 899–911.
- Rodríguez-Pérez, J.; Hamley, I. W.; Squires, A. M. **2010**, in preparation.
- Wei, F.; Zhang, D.; Halas, N. J.; Hartgerink, J. D. *J. Phys. Chem. B* **2008**, *112*, 9158–9164.
- Overman, S. A.; Aubrey, K. L.; Vispo, N. S.; Cesareni, G.; Thomas, G. J. *Biochemistry* **1994**, *33* (5), 1037–1042.
- Overman, S. A.; Thomas, G. J. *Biochemistry* **1995**, *34* (23), 7780–7780.
- De Gelder, J.; De Gussem, K.; Vandenabeele, P.; Moens, L. *J. Raman Spectrosc.* **2007**, *38* (9), 1133–1147.
- Lakowicz, J. R., *Principles of Fluorescence Spectroscopy*, 2nd ed.; Kluwer: Amsterdam, 1999.
- Smal, E. H.; Briza, P.; Panagos, A.; Berenfeld, L. *Infect. Immun.* **1995**, *63* (10), 4078–4083.
- Giri, K.; Bhattacharyya, N. P.; Basak, S. *Biophys. J.* **2007**, *92*, 293–302.
- Dafforn, T. R.; Rajendra, J.; Halsall, D. J.; Serpell, L. C.; Rodger, A. *Biophys. J.* **2004**, *86* (1), 404–410.
- Du, H.; Fuh, R. C. A.; Li, J. Z.; Corkan, L. A.; Lindsey, J. S. *Photochem. Photobiol.* **1998**, *68* (2), 141–142.
- Marshall, K. E.; Hicks, M. R.; Williams, T. L.; Hoffmann, S. V.; Rodger, A.; Dafforn, T. R.; Serpell, L. C. *Biophys. J.* **2010**, *98*, 330–338.
- Perkampus, H.-H., *UV-Vis Atlas of Organic Compounds*; VCH: Weinheim, 1992; Vol. 2.
- Du, H.; Fuh, R. A.; Li, J.; Corkan, A.; Lindsey, J. S. *Photochem. Photobiol.* **1998**, *68*, 141–142.
- Jung, J.-M.; Mezzenga, R. *Langmuir* **2010**, *26*, 504–514.
- Squires, A. M.; Devlin, G. L.; Gras, S. L.; Tickler, A. K.; MacPhee, C. E.; Dobson, C. M. *J. Am. Chem. Soc.* **2006**, *128* (36), 11738–11739.
- Zhang, S. G.; Holmes, T.; Lockshin, C.; Rich, A. *Proc. Natl. Acad. Sci. U.S.A.* **1993**, *90* (8), 3334–3338.
- Overman, S. A.; Thomas, G. J. *Biochemistry* **1995**, *34* (16), 5440–5451, erratum 7780.
- Overman, S. A.; Thomas, G. J. *Biochemistry* **1999**, *38* (13), 4018–4027.

JP101374E